JOURNAL OF SPACECRAFT AND ROCKETS
Vol. 38, No. 1, January–February 2001

Near-Field Measurement and Modeling Results for Flight-Type Arcjet: NH Molecule

Mark W. Crofton* and Teresa A. Moore†
The Aerospace Corporation, El Segundo, California 90245-4691
Iain D. Boyd‡
University of Michigan, Ann Arbor, Michigan 48109-2140
Ideo Masuda§
National Space Development Agency, Tsukuba, Ibaraki 305-8505, Japan
and
Yoshifumi Gotoh¶
Mitsubishi Electric Corporation, Kamakura, Kanaga 247, Japan

Density, velocity, and temperature data were obtained in the near-field plume of a 1.8-kW hydrazine arcjet thruster, using the NH molecule as a probe. This was the first laser spectroscopic study on a flight-type arcjet. The rotational temperature of NH was obtained in $v = 0, 1$ of the electronic ground state and the vibrational population in $v = 1, 2$. Rotational and vibrational temperatures were similar, and their variation along the thrust axis was minor. Line shapes as well as radial and axial profiles of the peak line intensity were obtained. Maximum laser-induced fluorescence signal was obtained on-axis 1.4 cm downstream from the exit plane, suggesting rapid NH production in the plume. Axial velocity components were determined at various plume locations. The power distribution of the available channels was found, on summation, to be in good agreement with arcjet input power. Direct simulation Monte Carlo predictions have been generated for comparison with much of the experimental data and to provide additional flowfield information. Good agreement was achieved in most cases.

Nomenclature

a	=	Gaussian normalization parameter, dimensionless
B_{12}	=	Einstein coefficient for absorption, $1 \rightarrow 2$
b	=	Gaussian linewidth parameter, cm^{-1}
E_{rot}	=	rotational energy of the originating state, cm^{-1}
f	=	oscillator strength, dimensionless
$g(\nu)$	=	Gaussian line shape function, dimensionless
I	=	intensity of photon flux
I_ν	=	intensity of photon flux at frequency ν
K	=	proportionality constant
M	=	species molar mass, amu
N_l	=	population density of lower level, cm^{-3}
n	=	species density, cm^{-3}
r	=	radial coordinate, cm
T	=	temperature, K
z	=	axial coordinate, cm
Δt_L	=	duration of laser pulse
$\Delta\nu$	=	full-width at half-maximum, cm^{-1}
ν	=	frequency, cm^{-1}
ν_0	=	center frequency, cm^{-1}
ρ	=	radiation density

Subscripts

D	=	Doppler
j, k	=	arbitrary energy levels of the ground electronic state
L	=	laser
P	=	power broadening
S	=	Stark effect
sa	=	self-absorption
sat	=	saturation

Received 13 December 1999; revision received 1 May 2000; accepted for publication 5 May 2000.

*Research Scientist, Space Materials Laboratory, Propulsion Science and Experimental Mechanics Department, M5-754, P.O. Box 92957, Los Angeles, CA 90009-2457. Member AIAA.

†Member of the Technical Staff, Space Materials Laboratory, Propulsion Science and Experimental Mechanics Department, MS-754, P.O. Box 92957, Los Angeles, CA 90009-2457.

‡Associate Professor, Department of Aerospace Engineering. Member AIAA.

§Assistant Senior Engineer, Data Relay Test Satellite Project Team, 2-1-1 Sengen.

¶Senior Engineer, Space Systems Department, 325, Kamimachiya.

Introduction

NORTH–SOUTH stationkeeping for the data relay test satellites (DRTS) being developed for launch around 2001 and the succeeding year will be provided by MR-509A/B hydrazine arcjet thrusters.[1] Despite the successful operation of PRIMEX Aerospace Corporation (PAC) arcjets on several U.S. satellites,[2] little quantitative information has been available concerning many of the thruster impacts on satellites of arbitrary configuration. To rectify this situation for the DRTS case, experimental measurements were performed and coupled with theoretical analyses. This resulted in the first laser-induced fluorescence and mass spectrometric studies for a flight-type arcjet thruster. A portion of the experimental work concerned with the measurement of near-field parameters is described in this report.

Near-field plume data are valuable for the understanding of the arcjet flow and performance properties. The study of spacecraft plume impingement and torquing, as well as contamination and thermal loading, are best accomplished via direct simulation Monte Carlo (DSMC) calculations. Validation and improvements in code accuracy are accomplished by incorporating the results of plume measurements into the modeling analysis.[3]

NH is a convenient probe species for vibrational, rotational, and translational temperatures in arcjets, as well as velocity and density distributions.[4,5] It has a readily accessible electronic transition originating from the ground state, with suitable lifetime, fluorescence, and linewidth properties.

Experimental Setup

Test Facility and Arcjet Operation

The experimental test chamber was 5.5 m in length with diameter of 2.4 m. Test chamber vacuum was maintained by 16 VHS-400 diffusion pumps. During thruster operation at the nominal flow rate

of 46.4 mg/s, test chamber background pressure was maintained below 1×10^{-3} torr.

The thruster was mounted on a computer-controlled four-axis positioning system. The arcjet nozzle was aligned with the long axis of the test chamber and remained there. The vertical position of the arcjet was similarly fixed for the duration of the measurements. Two-axis positioning was performed in the axial and radial directions to explore the spatial dependence of near-field parameters.

Electrical power of 1.8 kW was supplied at 80-V dc to a power conditioning unit (PCU) provided by PAC. Power was supplied at 28-V dc to operate the protection and control electronics, which were also provided by PAC. A flight-model PCU for DRTS, which would have required an input voltage of 33–51.5 V dc (Ref. 1), was not used.

A computer-controlled data acquisition and control system was supplied by The Aerospace Corporation and set up to satisfy PAC specifications regarding arcjet operating limits. Arcjet operating voltage, current, inlet pressure, and flow rates were monitored at all times, and an automatic shutdown would have occurred had any process limit been exceeded during normal operations. Typical recorded parameters at the 46.4-mg/s nominal operating point at which all H and NH data were obtained are 46.4-mg/s flow rate, 0.8-mtorr background pressure, 109.7-V arc voltage, 15.1-A arc current, 1.66-kW input power, 235-mN thrust, and 517 s I_{sp}, with the thrust and specific impulse estimated from data of Ref. 6. These quantities were reduced by 2% based on previous arcjet performance measurements comparing simulated N_2H_4 (2:1 mix of H_2:N_2) at ambient inlet temperature to catalytic decomposition of liquid N_2H_4 (Ref. 7). In practice, voltage and current levels varied somewhat but the power conditioner kept arcjet input power constant at 1.66 kW.

Laser-Induced Fluorescence

Laser-induced fluorescence (LIF) is the preferred means of obtaining the near-field parameters discussed in this report. The technique offers high spatial resolution together with high sensitivity and results that are acceptable from a quantitative standpoint. Submillimeter spatial resolution is a requirement in the near field because the arcjet nozzle width at the exit plane is on the order of a centimeter. Sensitivity is a factor at the existing species densities, which range from 10^{12} to 10^{16} cm^{-3} in the probed region.

For the NH data set, a one-photon absorption process was employed. In the limit of low laser power, the one-photon LIF signal intensity of a two-level system can be expressed as[8]

$$I = K N_l B_{12} \rho \, \Delta t_L \tag{1}$$

The constant K accounts for the details of the detection system and averaging of the laser field vector projection onto the transition dipole vector.

By determining relative quantum state populations, rotational and vibrational temperatures can be found. The relative populations of lower levels j and k may be found by using Eq. (1) to form the ratio

$$\frac{n_j}{n_k} = \frac{[B_{12}\rho\,]_k I_j}{[B_{12}\rho\,]_j I_k} \tag{2}$$

where any variation of detector response with frequency has been neglected. This equation is again valid in the limit of low laser power, but it holds for all cases where the laser power is the same for transitions from j and k, and the B coefficients for j and k are identical. Because the population is proportional to $(2J+1)\exp(-E_{\rm rot}/kT)$, the rotational temperature of the lower state can, in favorable cases, be determined from the relation

$$\ln[I/(2J+1)] \cong \ln C - E_{\rm rot}/kT \tag{3}$$

In the more general case for which laser pulse intensity is kept constant but the B coefficients vary over the series and the transitions are not fully saturated, $2J+1$ in Eq. (3) must be replaced by an expression depending on S_J, the line strength factor. Measurements of relative transition intensity for determination of rotational and vibrational temperature were made at pulse energy levels approaching the saturation limit (right side of Fig. 1), and temperatures were obtained without the use of line strength factors.

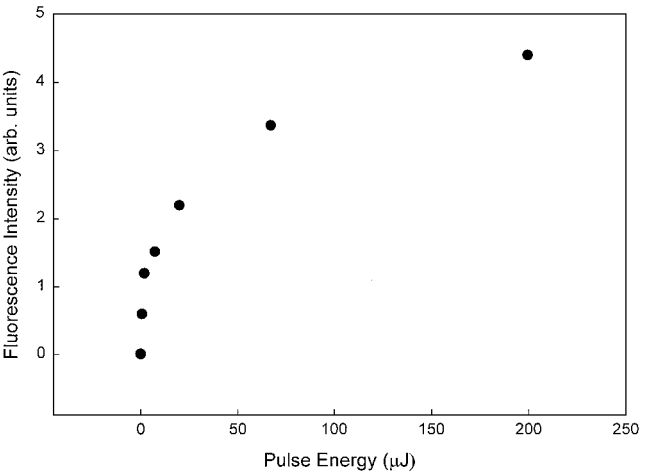

Fig. 1 Observed saturation effect of NH $R_2(7) v' = 0 \leftarrow v'' = 0$, $A\,^3\Pi \leftarrow X\,^3\Sigma^-$ transition.

Because of the large transition moment of the $A\,^3\Pi$–$X\,^3\Sigma^-$ transition ($f = 0.0075$) (Ref. 9), the <10-ns duration of the laser pulse and the requirement of submillimeter spatial resolution, it was difficult to eliminate all saturation effects. A measurement of LIF signal intensity from NH over a range of laser pulse energies produced the curve given in Fig. 1. The saturation effect is obvious. For each data point, pulse energy was measured near the output of the dye laser harmonic doubler. Energy levels at the arcjet itself were approximately 60% of these values.

Because of power broadening, the linewidth of NH transitions will be proportional to $(1 + I/I_{\rm sat})^{1/2}$ (Ref. 10). The width of $R_2(7)$ was broadened to 0.4 cm^{-1} at ≈200-μJ pulse energy levels. Pulse energy was ≈4 μJ for the measurement of peak signal profile along the thrust axis, and composite parallel and perpendicular line shapes. Pulse energy was kept constant for the measurements of relative rotational line strength. For the latter data, pulse energy was about 20 μJ. Given the small variation in B coefficients and saturation of the transitions, $2J+1$ was used in Eq. (3) for the temperature determinations, rather than S_J.

Quenching of excited states may occur as a result of collisions with partners in other quantum states. Quenching is usually a problem at high gas densities. For the arcjet, the sum of species densities at the nozzle exit plane is about 1×10^{16} cm^{-3}. In LIF measurements, if the upper state lifetime is much shorter than the interval between quenching collisions, quenching effects can be neglected. The NH molecule has a lifetime in the $A\,^3\Pi$ excited state of about 400 ns (Refs. 11 and 12). During an interval of 400 ns, NH molecules moving along the plume axis at 7 km/s travel 2.8 mm. The laser beam was positioned to traverse the plume 1–2 mm upstream from the center of the detection zone, to reduce the detected laser scatter. With an effective detection-zone length for NH fluorescence of about 2 mm, NH fluorescence would be largely detected between 100 and 350 ns after initial excitation. This interval was reduced by the boxcar gate, set to span 100–280 ns after the laser pulse. The interval between quenching collisions of an NH molecule with the background gas near the nozzle exit plane is on the order of 1 μs, so that quenching can have some influence on the observed fluorescence. Substantial quenching effects are to be expected inside the nozzle.

A YAG-pumped dye laser operating at 40-Hz repetition rate generated ≥1 mJ per 6-ns pulse in the 660–680-nm region, using a DCM/LD700 dye mixture. The dye laser output was doubled in a KDP crystal, which was tuned in the 330–340-nm range. A tracking circuit maintained maximum output despite temperature drifts and frequency tuning.

After elevation to the appropriate height for entry into the vacuum chamber, the laser beam entered through a window and passed through the arcjet plume perpendicular to the arcjet thrust axis as shown in Fig. 2. To obtain an axial velocity measurement, an optic placed below the thruster steered the beam to a second optic sitting downstream and below the thrust axis. The latter optic steered the beam to intersect the plume at an angle of 43 deg with respect to

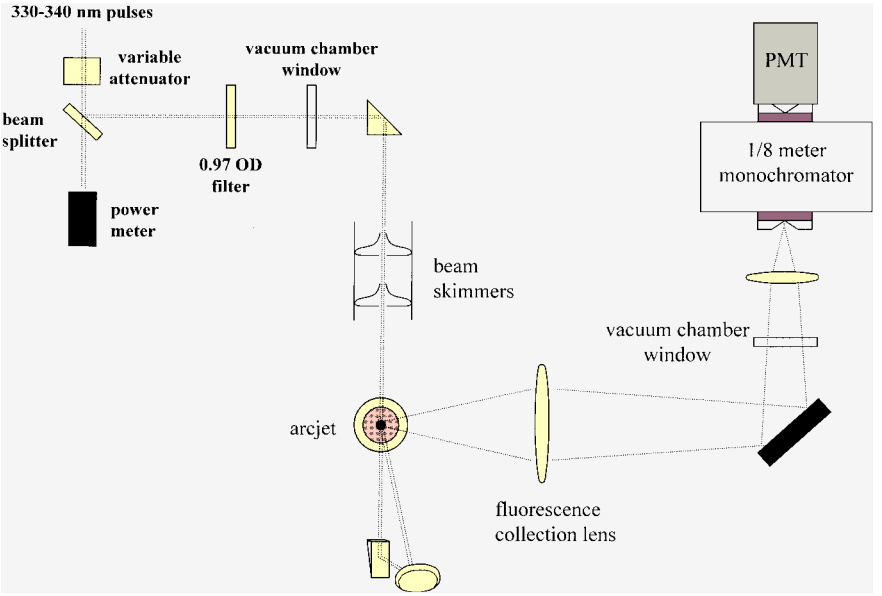

Fig. 2 Schematic for part of the experimental setup.

the thrust axis and in the correct location to be aligned with the fluorescence collection optics.

For NH, the laser beam was weakly focused to enhance the spatial resolution. Resonant fluorescence was collected by a 5-cm-diam MgF_2 lens placed 18 cm away from the arcjet centerline. The slowly converging fluorescence beam was transmitted over a distance of 1.2 m to a reflector that steered it through an LIF window into the external environment. The fluorescence beam then entered a 0.125-m monochromator. Detection was accomplished by means of a Hamamatsu R955 photomultiplier tube attached at the monochromator exit. A boxcar amplifier was used to integrate the signal. Alignment of the collection optics was accomplished using a HeNe laser propagated back from the monochromator entrance or scattered light from the probe laser at the location of interest.

The laser pulse energy generating the fluorescence was recorded together with the fluorescence signal using computerized data acquisition. NH data were usually taken at a constant average energy level, maintained over the frequency range of interest through the use of an attenuator (polarizer half wave plate combination). NH data were not normalized for power dependence because this was not deemed necessary, and for measurements at higher power levels the power dependence was highly nonlinear. Further attenuation of the pulse energy was required when measuring radial and axial signal profiles and line shapes. A beamsplitter and neutral density filter combination reduced the pulse energy by an additional factor of $\sim$30 for line shapes and axial intensity profiles. Copper sheet was placed over the aluminum thermal shield beneath the arcjet to reduce the level of scattered light. Scattering was a problem for measurement of the axial intensity profile before installing the copper sheet and attenuating the laser beam.

Line shapes were obtained by stepping the dye laser frequency, collecting signal for a suitable period, and repeating over the full range of the transition. Fundamental frequencies were obtained in vacuum wave numbers using a pulsed wavemeter, with typical relative accuracy of 0.01–0.02 cm^{-1}. Data are, therefore, plotted against the dye laser fundamental, with the laser frequency of the experimental measurements obtained by doubling the value shown. The wavemeter was automatically calibrated at intervals with an internal helium–neon laser, but was subject to minor drifting behavior between calibrations, which occasionally resulted in readout errors of up to 0.03 cm^{-1}. Line shapes were fitted with a three-parameter Gaussian function:

$$g(\nu) = a \exp\left\{-\tfrac{1}{2}[(\nu - \nu_0)/b]^2\right\} \tag{4}$$

In many cases the transition center frequency was fixed, but the linewidth parameter and peak height were always variables. These parameters normally showed little dependence on whether the center frequency was fixed. The small residual baseline present in the experimental measurements was subtracted prior to fitting.

The linewidth was determined largely by Doppler broadening and laser linewidth. In a few cases power broadening was suspected or known to be large. Those data are not included in this report. The Doppler width [full width at half maximum (FWHM)] is determined by the Maxwell–Boltzmann distribution and is related to temperature by

$$\Delta\nu_D = 2\sqrt{2\,\ell n 2}\, b_D = 7.162 \times 10^{-7} \nu_0 \sqrt{T/M} \tag{5}$$

where

$$b_D \cong \sqrt{b^2 - b_L^2 - b_S^2 - b_{\mathrm{sa}}^2 - b_P^2} \tag{6}$$

Because Stark broadening, self-broadening, and power broadening do not give rise to a Gaussian line shape, Eq. (6) is an approximation only applicable where b_S, b_{sa}, and b_P are effective widths and $b_{\mathrm{sa}}^2, b_S^2, b_P^2 \ll (b_D^2 + b_L^2)$. The translational temperature (Kelvin) may be expressed as

$$T = 1.0811 \times 10^{13} \left(M \big/ \nu_0^2\right) b_D^2 \tag{7}$$

The linewidth (FWHM) at the dye-laser fundamental frequency was assumed to be 0.05 cm^{-1} and Gaussian, in approximate agreement with the dye laser specifications and width of the wavemeter etalon fringes. The laser linewidth at the doubled dye laser frequency was assumed to be 0.07 cm^{-1} (0.035 cm^{-1} for plots using the fundamental frequency).

Following the application of line broadening and quenching corrections, the H atom experimental density profile was in acceptable agreement with the DSMC result.[13] For NH, the difference between the DSMC result and the experimental result is still nearly an order of magnitude after accounting for linewidth and quenching effects.

Quenching of the NH excited state by the background of molecules and atoms in the plume is nonnegligible. The rates of quenching by H_2 and N_2 at 1400 K have been measured,[14] with the respective rate constants 1.9×10^{-10} and $<2\times10^{-12}$ $cm^3\ s^{-1}$. The quenching rate by H atom is probably $\geq 1.7\times10^{-10}$ $cm^3\ s^{-1}$ at room temperature.[15] Assuming a $T^{1/2}$ dependence for these rate constants at the elevated temperature of the arcjet, quenching by H atom and H_2 occurs at similar rates with the combined rate of 2×10^6 s^{-1}, about equal to the rate of radiative decay. That quenching does occur in the plume was verified by the observed decrease in fluorescence decay time near the nozzle exit plane. At the usual boxcar gate setting

of 100-ns delay and 180-ns width, the fluorescence decay rate was observed to increase within 3 mm of the exit plane, on centerline. Because the optical alignment spatially limited the detection window for fluorescence, the full fluorescence decay curve could not be observed. It is believed that the effect of quenching on data obtained $\geq$3 mm from the exit plane was small.

The error in individual data points for linewidth measurements is reflected by their deviations from the Gaussian fitting function because the measurements were relative rather than absolute. For radial and axial profiles of peak signal intensity, the error can similarly be inferred from deviations of individual data points from a least-squares-fitting function or from the scatter between adjacent points in regions of low curvature.

Numerical Approach

The flow inside the hydrazine arcjet is characterized by relatively low densities and very high temperatures. The Knudsen number of the nozzle flow (ratio of mean free path to boundary-layer scale) varies from about 0.001 at the nozzle throat to about 0.1 at the nozzle exit plane. These values indicate that the flow will be in a state of thermochemical nonequilibrium. At the same time, on the flow axis near to the arc constriction, the ionization level can be as high as 40% (Ref. 16).

These conditions place a heavy demand on attempts to perform accurate numerical simulations of the arcjet flow. At PAC, a continuum-based computer code called KARNAC has been developed for computing arcjet flows. The code has performed very well in detail for hydrogen arcjet flows.[17] The accuracy of the code for hydrazine flows is less clear. There are several physical limitations of the KARNAC code. First, all energy modes are assumed to be in equilibrium, precluding the possibility of freezing of the vibrational and rotational energy modes of the molecular species in the flow (N_2 and H_2). These are known to be loss mechanisms for arcjets. Second, by the time a Knudsen number of 0.1 is reached, the physical basis of the Navier–Stokes equations of fluid mechanics is no longer valid. Finally, because there is no thermal nonequilibrium included, important physical phenomena such as vibration–dissociation coupling are missing.

Although we are primarily interested in analysis of the arcjet plume, for the reasons just listed, a more detailed analysis of the nozzle flow is also merited. In the present study, the DSMC method[18] is employed to compute both the nozzle and plume flows in a single simulation. The nozzle flow is begun just downstream of the constrictor in a region of the flow that is in the continuum regime. A startline for the DSMC computation is obtained from a solution generated by KARNAC and provided by PAC. The DSMC code includes the following physical phenomena: 1) multispecies flow (H_2, H, H^+, e^-, N_2, and N), 2) rotational and vibrational relaxation, 3) dissociation (with vibration coupling), ionization, and recombination reactions, and 4) ohmic heating. The code is described in detail[16] and has been extensively validated against experimental data for hydrogen arcjets.[19]

In terms of boundary conditions, the nozzle wall is treated as being diffuse with full accommodation of all energy modes to a fixed temperature of 1400 K. For the plume expansion, the experimentally determined backpressure of 0.113 Pa is imposed. The analysis is performed for the nominal operating case of a flow rate of 46.4 mg/s and a power input to the arcjet of 1660 W.

The computation employs a structured grid of 500 × 70 cells. At steady state, a total of about 350,000 particles is employed. The computations provide mean particle quantities such as density, temperature, and velocity. Velocity distribution functions are also computed, and this required the simulations to be performed over an extended period to reduce statistical scatter in the distributions collected.

Results and Discussion

The mass spectrometry data indicated N and NH mole fractions in the far field of 6 and 1.5%, respectively.[20] NH was left out of the simulations, which substantially underestimated N abundance. NH was not included in the DSMC calculations due to its chemistry and low abundance relative to N_2. In retrospect it would have been useful for NH to be included in the simulations. Theoretical and experimental comparisons are performed between DSMC data for nitrogen atom and LIF data for the NH molecule because NH and N velocity and density distributions will be similar in the absence of chemical effects.

The line shapes obtained for NH are plotted in Fig. 3, along with their Gaussian fits. In each case the laser beam intersected the plume centerline at an angle of about 42.8 deg, resulting in a composite of perpendicular and parallel line shapes. The line shape peaks are red shifted about 0.22 cm^{-1} from the known transition frequency of $R_2(7)v' = 0 \leftarrow v'' = 0$, because of the NH Doppler shift at its axial plume velocity.

The temperatures indicated in Table 1 were obtained from the relation

$$\Delta\nu \cong \sqrt{\Delta\nu_D^2 + \Delta\nu_L^2 + \Delta\nu_P^2} \tag{8}$$

and Eqs. (5–7). Doppler broadening largely determines the line shape when the laser pulse energy is low. For the conditions of the experiment, the contribution of power broadening to the linewidths was roughly estimated at 7%. In contrast to the H atom, the dc Stark (see Ref. 21) and collisional Stark effects for NH are relatively small and were neglected in the analysis. Self-absorption was also neglected because no evidence of it was observed.

Table 1 NH parallel and perpendicular translational temperatures from DSMC and experimental data

(r, Z), cm	Perpendicular temperature, K DSMC (N atom)	Parallel temperature, K DSMC (N atom)	Composite temperature, K DSMC (N atom)	Composite temperature, K experiment (NH)
0, 0.18	1700	3620	2730	3060 ± 400
0, 1.96	620	2410	1580	2420 ± 400

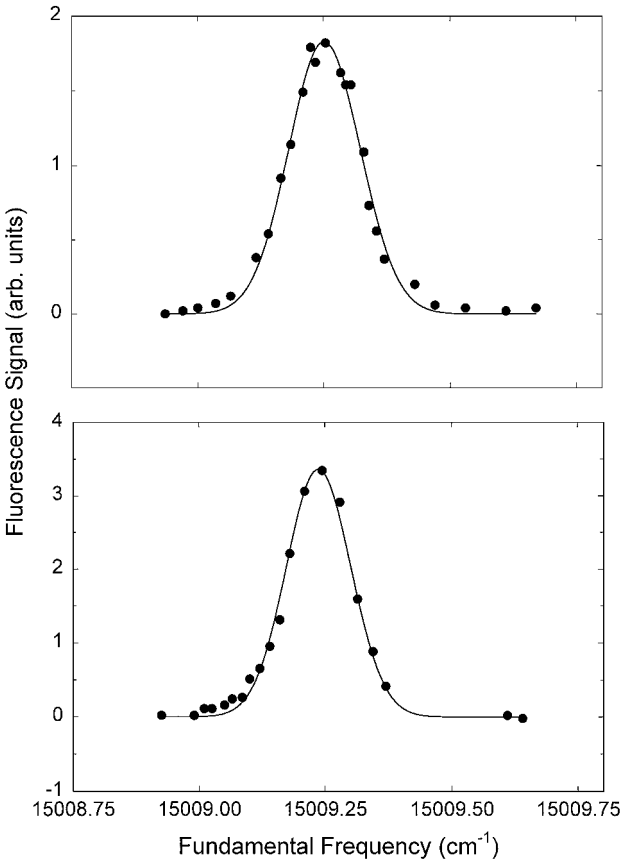

Fig. 3 NH line shapes for $R_2(7)$ 0–0 obtained on centerline at z = 0.18 cm (top) and 1.96 cm (bottom); transition frequency is 30,018.936 cm^{-1}, absent a Doppler shift.

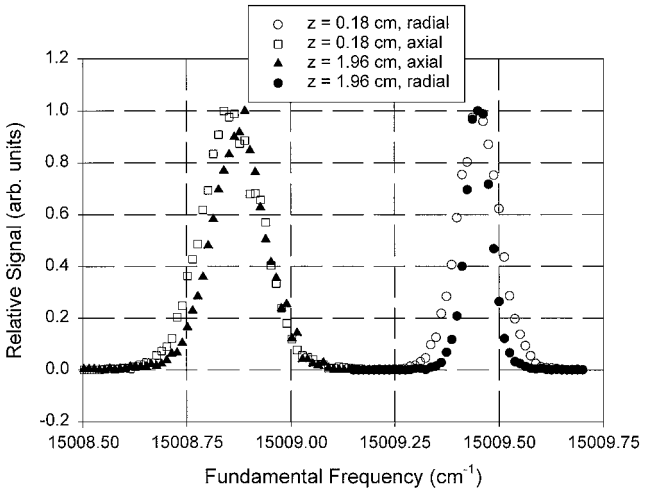

Fig. 4 N atom parallel (radial) and perpendicular (axial) line shapes for $R_2(7)$ 0–0 from DSMC results.

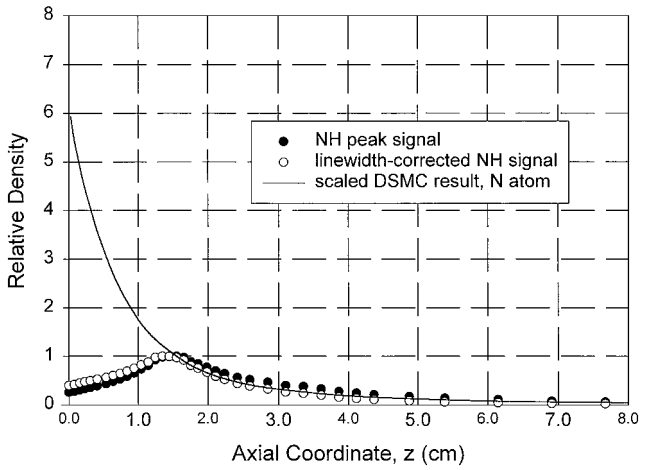

Fig. 5 NH and N atom profiles on centerline, from experimental and DSMC data, respectively.

The N atom parallel and perpendicular line shapes obtained by the DSMC method are plotted in Fig. 4. The perpendicular line shapes are those predicted for the case in which the probe laser is along the axis of thrust. The temperatures corresponding to each line shape are included in Table 1. A direct comparison between parallel and perpendicular temperatures for DSMC and experimental data could not be made because all of the parallel line shapes in the experimental data set were believed to be substantially power broadened.

The peak LIF signal at the center of the line shape was measured as a function of axial coordinate, on centerline, and is plotted in Fig. 5. Data were obtained out to about 8 cm, where the source density is approaching the background density of the test chamber. Like the hydrogen atom case, the axial dependence of peak signal is nonmonotonic. The NH signal peaks at 1.4 cm downstream from the exit plane, whereas H atom signal peaked at 0.8 cm. The unexpected existence of such a prominent peak at $z = 1.4$ cm may result from a high production rate of NH at this location. An NH formation rate on the order of 10^{19} cm^{-3} s^{-1} is anticipated near the exit plane, which can create the required 10^{13} cm^{-3} population density within 1 μs.

The DSMC density profile for N atom is also shown in Fig. 5 for comparison. The DSMC result gives density directly, so that for direct comparison the experimental result should be multiplied at each data point by the corresponding radial linewidth. The linewidth-corrected profile obtained from applying DSMC linewidth factors is also shown in Fig. 5. Quenching is estimated to further account for about a factor of two correction, but a large discrepancy remains. As already mentioned, the most plausible explanation is the rapid formation of NH directly in the plume, such that the centerline density actually increases from the exit plane to $z = 1.4$ cm despite the geometric plume expansion.

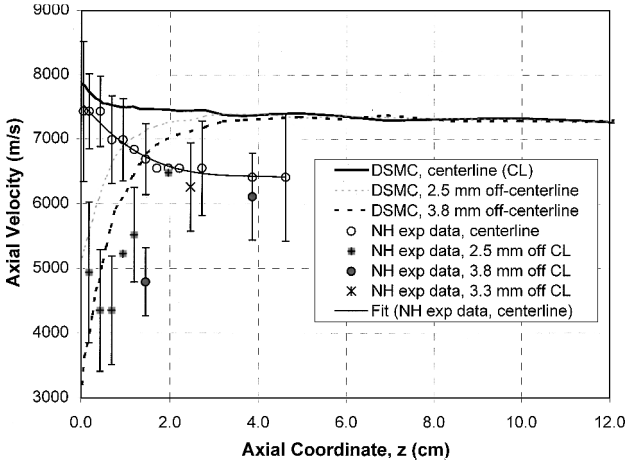

Fig. 6 Comparison of experimental (symbols) and DSMC data (lines) for peak axial velocity component.

The peak of the measured axial velocity distribution, in meters per second, is plotted in Fig. 6. Figure 6 also indicates the DSMC results obtained for N atom. A reduction in peak flow velocity occurs with increasing distance from the exit plane, on centerline, in each case. The experimental peak velocity is 0.3–1 km/s lower and appears to indicate a larger velocity decrease with distance from the exit plane. The peak velocity decreases more abruptly with radial than with axial coordinate, as expected, but the radial drop of the experimental data is faster than the DSMC result would predict. This could contribute to error in the DSMC radial density profile, particularly near the exit plane. Estimates of the experimental absolute error limits are shown for selected data points. The uncertainty stems from errors in the wavemeter reading, in locating the center of the transition, and in the optical alignment. These DSMC results are consistent with the mass spectrometry data for N atom.[3,20] However, the far-field DSMC result used in the DRTS impingement model[3] was about 7.0 km/s on the centerline for species containing nitrogen, and the specific impulse and thrust figures resulting from the mass spectrometry data[20] were 15% higher than the thrust stand numbers.[6,20] These observations suggest that the present LIF result of a 6.4-km/s limit for NH at $z \geq 4$ cm is accurate and does not contain a systematic error.

NH is left with substantial internal and translational energy as a byproduct of most mechanisms that form it in the arcjet plume. Mechanisms of formation that operate at substantial rates and may leave residual energy in the NH product include dissociative electron impact, dissociative electron recombination, bimolecular reaction, and photolysis.[15,22,23] Normally, one would expect that ground state species are relatively equilibrated with the translational and rotational degrees of freedom in the background gas. This is probably the case for NH, with excited states in nonequilibrium with each other and the ground state.[4,24] In the extreme case, even the velocity distribution of an excited state can be in nonequilibrium.[25]

Because NH is relatively massive, its velocity distribution will tend to be widened by collisions with the relatively fast, abundant species of H and H_2. This process leads to a DSMC rotational temperature for N_2 greater than 4000 K, with the H_2 rotational temperature about 2000 K lower, as shown in Fig. 7. The vibrational temperatures are predicted to follow similar trends, according to the DSMC results. The rotational temperature of NH was studied in $v = 0$, 1 of the ground electronic state. The relative intensities of $Q_2(J)$ and $R_2(J)$ series were measured, keeping laser intensity a constant. No difference was found between $v = 0$ and 1 rotational temperatures, to within experimental error. A slow drop in rotational temperature with z is believed to exist because the trend is also indicated by the DSMC data. The plots of Fig. 8 were made according to Eq. (3), and approximately yield the temperatures given in Table 2.

The upper state lifetime depends on vibrational state as well as rotational state, although the best experimental and theoretical results

Table 2 NH rotational and vibrational temperatures (Kelvin)

(r, Z), cm	Rotational, $v'' = 0$		Vibrational	
	$Q_2(J)$ series	$R_2(J)$ series	(1–1)/(0–0)	(2–2)/(0–0)
0, 0.18	2980 ± 290	2800 ± 500	2750 ± 200	3090 ± 400
0, 0.94	2750 ± 250	——	——	——
0, 1.96	2690 ± 160	——	2720 ± 200	2780 ± 300
0, 4.11	——	——	2570 ± 300	——

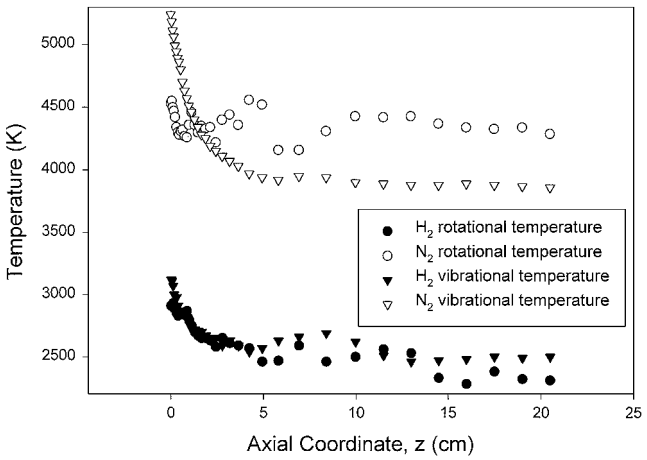

Fig. 7 DSMC results for rotational and vibrational temperatures of H_2 and N_2.

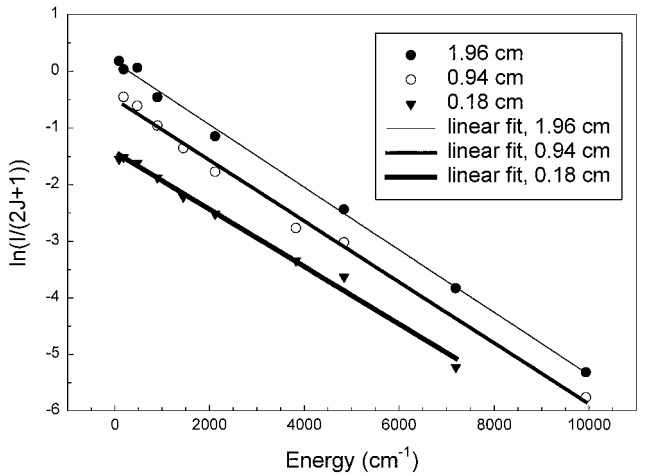

Fig. 8 Rotational temperature determinations using the experimental data and Eq. (3).

differ.[11,12] Using the radiative and predissociative rates of the theoretical computations, which are probably the best available, resulted in small rotational temperature corrections on the order of 100 K, which are reflected in the values of Table 2. The corrections were smaller than the experimental uncertainty and are themselves approximate due to the uncertainty in radiative and predissociative rates and the spatially dependent quenching rate.

Vibrational temperature was also determined, from the ratio of 2–2 and 1–1 transitions to 0–0. These transitions are known to have similar oscillator strengths, except that the 2–2 case suffers from predissociation in the upper state, which reduces the state lifetime. Corrections were made reflecting the predissociation effect. The vibrational and rotational temperatures were found to be remarkably similar.

Radial profiles of peak signal intensity are plotted in Fig. 9. These were converted to density profiles using the DSMC velocity distribution functions for the N atom, along the radial cuts. The result in shown in Fig. 10. Excellent agreement was obtained at $z = 1.96$ and 3.23 cm, but it is apparent that the experimental profile at $z = 0.30$ cm

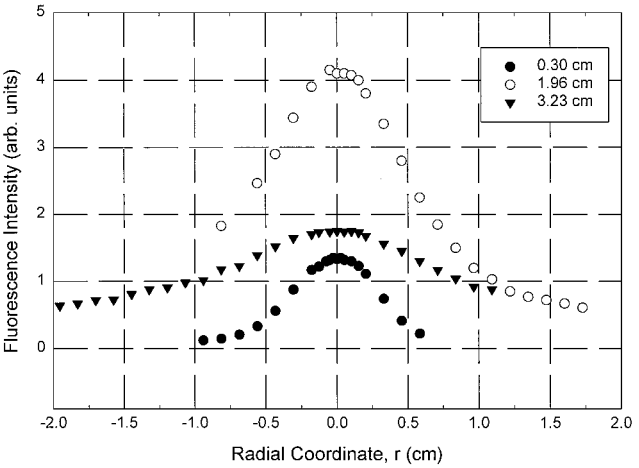

Fig. 9 NH radial profiles of peak LIF intensity.

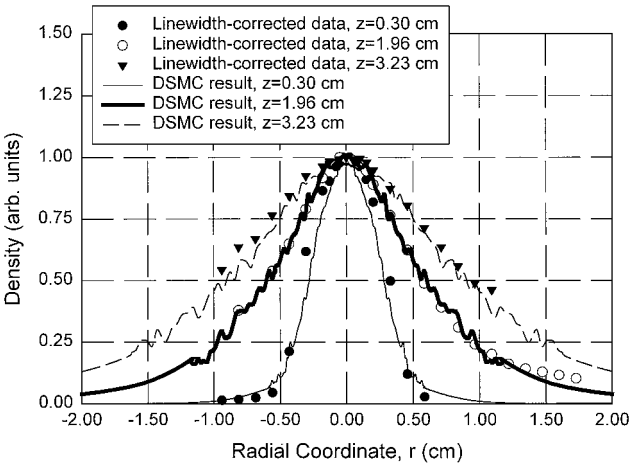

Fig. 10 DSMC radial density profiles for nitrogen atom (lines), compared to linewidth-corrected NH experimental data (symbols).

is slightly wider than the DSMC profile. This can be explained as a quenching effect, which flattens the peak with respect to the shoulders, and/or as an error in the DSMC density profile (see Fig. 6 and discussion pertaining to it).

From the dissociation fraction of H_2 or the absolute density of H atoms determined elsewhere,[20,26,27] one of the major power loss mechanisms of the arcjet can be estimated. The dissociation fraction determined by mass spectrometry was 14.3% (Ref. 20). At the 6.0-mg/s flow rate of H_2, the flow rate of dissociated molecules is 2.6×10^{20} s^{-1}, corresponding, at 4.48 eV/mol, to a power loss of 184 W. For N_2, the far-field dissociation fraction is 10.9%, corresponding to a flow rate of dissociated molecules equal to 9.5×10^{19} s^{-1} and, at 9.76 eV/mol, a power loss of 148 W. Dissociation, therefore, accounts for 20% (332 W/1660 W) of the total arcjet power input. This is a much smaller percentage than the 64% that has been proposed recently for the hydrogen arcjet.[27]

Other power losses include thermal conduction and radiation (across the entire spectrum), molecular rotation and vibration, and electronic excitation and ionization. On the basis of the available MR509A data, each of these can now be estimated because we have useful knowledge concerning the rotational, translational, and vibrational temperatures of all major species, ionization and excitation fractions, mole fractions, etc. The estimated power sinks (watt) for the MR 509A at the 1660-W, 46.4-mg/s operating point were $184 + 148 = 332$ molecular dissociation, 60 transverse thermal kinetic (not measured by mass spectrometry), $60 + 60 = 120$ molecular rotation and vibration, 160 thermal conduction and radiation (approximately 10% of the total arcjet input power, see Ref. 25), 430 ± 170 waste kinetic power (difference between measured

kinetic power obtained from mass spectrometry and thrust power derived from thrust stand measurement), and 10 ionization and excitation. Thermal radiative loss from the arcjet body is typically about 10% of the arcjet input power,[28] and conductive loss is relatively minor for a properly designed test setup. Convective heat loss can be neglected at the background pressure of this experiment. Plume radiative losses over the entire spectrum are negligible in comparison to the radiative losses from the arcjet body.[29] The sum of all nontranslational power sinks is about 590 W. The kinetic power flux determined by mass spectrometry was 1007 ± 171 W (Ref. 20). The direct measurement of arcjet thrust on the standard MR509 arcjet came up with 580-W thrust power.[6,20] Taking the average and subtracting from 1007, 427 ± 171 W of waste kinetic power is obtained, assuming the error bars are small for the direct thrust measurement. The angular and species dependence of the velocity and mass flux distribution functions is believed to be the major source of kinetic power, which does not produce useful thrust. The data reveal a very broad width for the average speed distribution of the collection of atoms and molecules.[20] In addition, velocity distributions (with their associated kinetic energy) transverse to the arcjet-detector axis are not reflected in the 1007-W figure because the mass spectrometer does not detect them. The experimental uncertainty associated with the total waste kinetic power is high, but nonuseful kinetic power is obviously one of the largest single categories for arcjet power loss. Adding all of the sinks together, we have a sum of about 1690 W, which is in good agreement with the arcjet input power. This is the first time that total power losses have been determined to this level of accuracy or that the sum has been in close agreement with the known power input.

The discrepancy in H atom density values obtained for the hydrogen arcjet from DSMC results and the experimental approach of Ref. 27 may now be resolved. The DSMC result, which is more consistent with other modeling calculations and a previous experimental measurement of dissociation fraction in a hydrogen arcjet,[30] is the more accurate one. The more recent experimental dissociation fraction of H_2, determined by Wysong and Pobst,[27] was too high, but the neglect of most of the waste kinetic power as in previous analyses[4,31] reduced the discrepancy in the computed power balance.

Conclusions

Temperature, velocity, and relative density measurements were obtained in the simulated hydrazine arcjet plume using the NH molecule as probe species. Experimental and theoretical plume data, comparing NH experimental and N atom theoretical results, were in generally good agreement for a flight-type hydrazine arcjet. Agreement between theory and experiment was especially good for the radial density profiles, except near the exit plane. Close agreement was also obtained for the axial density profile, except near the exit plane, where the discrepancy is large. Rapid production of NH near the exit plane is proposed to fit this observation. In a comparison of the measured NH and computed N peak axial velocity component, the experimental velocity dropped more quickly with distance off centerline. The centerline velocity several centimeters from the exit plane was 15% lower than the DSMC prediction.

An analysis of the arcjet power distribution among the various sinks reveals that molecular dissociation and waste kinetic power produce the largest losses. The expended kinetic power not producing useful thrust is a larger quantity than has been previously appreciated. Using the figures available for the various sinks, which are generally more accurate than previous values, good agreement has now been obtained between the sum and the known power input.

A positive synergy between experiment and theory has been useful in furthering the fundamental understanding of the arcjet. A comprehensive picture is beginning to emerge regarding the atomic and molecular energy distribution for all available modes throughout the arcjet plume.

Acknowledgments

Thruster operations support was provided by D. Zube, J. English, and S. Crook of PRIMEX Aerospace and J. Pollard, M. Worshum, L. Ortega, and E. Fournier of The Aerospace Corporation. E. Beiting, J. Pollard, and R. Cohen provided valuable assistance in other aspects of the project. This manuscript is a revision of a 1998 report to Mitsubishi Electric Corporation (MELCO). The original work was done under Contract to MELCO during 1997–1998. Preparation of the revised manuscript was partially funded by The Aerospace Corporation Independent Research and Development program.

References

[1]Zube, D. M., Fye, D., Masuda, I., and Gotoh, Y., "Low Bus Voltage Hydrazine Arcjet System for Geostationary Satellites," AIAA Paper 98-3631, July 1998.

[2]Martinez-Sanchez, M., and Pollard, J. E., "Spacecraft Electric Propulsion," *Journal of Propulsion and Power*, Vol. 14, No. 5, 1998, pp. 688–699.

[3]Nelson, D. A., Gotoh, Y., and Masuda, I., "A Simplified Model for the Prediction of Arcjet Plumes," IEPC Paper 99-043, Oct. 1999.

[4]Crofton, M. W., Welle, R. P., Janson, S. W., and Cohen, R. B., "Temperature, Velocity and Density Studies in the 1 kW Ammonia Arcjet Plume by LIF," AIAA Paper 92-3241, July 1992.

[5]Brazier, C. R., Ram, R. S., and Bernath, P. F., "Fourier Transform Spectroscopy of the $A\,^3\Pi$-$X\,^3\Sigma^-$ Transition of NH," *Journal of Molecular Spectroscopy*, Vol. 120, No. 2, 1986, pp. 381–402.

[6]Smith, R. D., Roberts, C. R., Aadland, R. S., Lichtin, D. A., and Davies, K., "Flight Qualification of the 1.8 kW MR-509 Hydrazine Arcjet System," International Electric Propulsion Conf., IEPC Paper 97-081, Aug. 1997.

[7]Morren, W. E., and Lichon, P. J., "Low-Power Arcjet Test Facility Impacts," AIAA Paper 92-3532, July 1992.

[8]Altkorn, R., and Zare, R. N., "Effects of Saturation on Laser-Induced Fluorescence Measurements of Population and Polarization," *Annual Review of Physical Chemistry*, Vol. 35, 1984, pp. 265–89.

[9]Smith, W. H., and Liszt, H. S., "Franck–Condon Factors and Absolute Oscillator Strengths for NH, SiH, S_2, and SO," *Journal of Quantitative Spectroscopy and Radiative Transfer*, Vol. 11, No. 1, 1971, pp. 45–54.

[10]Citron, M. L., Gray, H. R., Gabel, C. W., and Stroud, C. R., Jr., "Experimental Study of Power Broadening in a Two-Level Atom," *Physical Review A*, Vol. 16, No. 4, 1977, pp. 1507–1512.

[11]Smith, W. H., Brzozowski, J., and Erman, P., "Lifetime Studies of the NH Molecule: New Predissociations, the Dissociation Energy, and Interstellar Recombination," *Journal of Chemical Physics*, Vol. 64, No. 11, 1976, pp. 4628–4633.

[12]Patel-Misra, D., Parlant, G., Sauder, D. G., Yarkony, D. R., and Dagdigian, P. J., "Radiative and Nonradiative Decay of the NH(ND) $A\,^3\Pi$ Electronic State: Predissociation Induced by the $^5\Sigma^-$ State," *Journal of Chemical Physics*, Vol. 94, No. 3, 1991, pp. 1913–1922.

[13]Crofton, M. W., Moore, T. A., Boyd, I. D., Masuda, I., and Gotoh, Y., "Near-Field Measurement and Modeling Results for a Flight-Type Arcjet: H Atom," International Electric Propulsion Conf., IEPC Paper 99-048, Oct. 1999.

[14]Garland, N. L., Jeffries, J. B., Crosley, D. R., Smith, G. P., and Copeland, R. A., "NH $A\,^3\Pi_i$ Quenching at 1400 K," *Journal of Chemical Physics*, Vol. 84, No. 9, 1986, pp. 4970–4975.

[15]Dodd, J. A., Lipson, S. J., Flanagan, D. J., Blumberg, W. A. M., Person, J. C., and Green, B. D., "NH ($X\,^3\Sigma^-$, v = 1–3) Formation and Vibrational Relaxation in Electron-Irradiated $Ar/N_2/H_2$ Mixtures," *Journal of Chemical Physics*, Vol. 94, No. 6, 1991, pp. 4301–4310.

[16]Boyd, I. D., "Monte Carlo Simulation of Nonequilibrium Flow in Low Power Hydrogen Arcjets," *Physics of Fluids*, Vol. 9, No. 10, 1997, pp. 3086–3095.

[17]Butler, G. W., Boyd, I. D., and Cappelli, M. A., "Nonequilibrium Flow Phenomena in Low Power Hydrogen Arcjets," AIAA Paper 95-2819, July 1995.

[18]Bird, G. A., *Molecular Gas Dynamics and the Direct Simulation of Gas Flows*, Oxford Univ. Press, Oxford, 1994.

[19]Boyd, I. D., "Extensive Validation of a Monte Carlo Model for Hydrogen Arcjet Flow Fields," *Journal of Propulsion and Power*, Vol. 13, No. 6, 1997, pp. 775–782.

[20]Pollard, J. E., Masuda, I., and Gotoh, Y., "Plume Mass Spectrometry and Calorimetry with a Hydrazine Arcjet Thruster," International Electric Propulsion Conf., IEPC Paper 99-041, Oct. 1999.

[21]Irwin, T. A. R., and Dalby, F. W., "Experimental Determination of the Dipole Moments of the Degenerate States of NH," *Canadian Journal of Physics*, Vol. 43, No. 10, 1965, pp. 1766–1775.

[22]Tokue, I., Fujimaki, A., and Ito, Y., "Formation and Internal Energy Distributions of the NH (A,c) Radicals by Electron-Impact Dissociation of Hydrazine and Methylamine," *Journal of Physical Chemistry*, Vol. 88, No. 25, 1984, pp. 6250–6254.

[23]Haak, H. K., and Stuhl, F., "ArF (193 nm) Laser Photolysis of HN_3, CH_3NH_2, and N_2H_4: Formation of Excited NH Radicals," *Journal of Physical Chemistry*, Vol. 88, No. 16, 1984, pp. 3627–3633.

[24]Zube, D. M., and Myers, R. M., "Thermal Nonequilibrium in a Low-Power Arcjet Nozzle," *Journal of Propulsion and Power*, Vol. 9, No. 4, 1993, pp. 545–552.

[25]Kurawake, J., and Ogawa, T., "Translational Energy Distributions and Production Mechanisms of the Excited Hydrogen Atom (n = 3, 4) Produced in e-NH3 Collisions," *Chemical Physics*, Vol. 86, 1984, pp. 295–301.

[26]Pollard, "Arcjet Diagnostics by XUV Absorption Spectroscopy," AIAA Paper 92-2966, July 1992.

[27]Wysong, I. J., and Pobst, J. A., "Quantitative Two-Photon Laser-Induced Fluorescence of Hydrogen Atoms in a 1 kW Arcjet Thruster," *Applied Physics B*, Vol. 67, No. 2, 1998, pp. 193–205.

[28]Janson, S. W., "The Impact of Advanced Diagnostic Techniques on Electrothermal Thruster Design," AIAA Paper 92-3242, July 1992.

[29]Crofton, M. W., "Spectral Irradiance of the 1 kW Arcjet Thruster from 80 to 500 nm," AIAA Paper 92-3237, July 1992.

[30]Pollard, J. E., "Arcjet Diagnostics by XUV Absorption Spectroscopy," AIAA Paper 92-2966, July 1992.

[31]Fujita, K., "Performance Computation of a Low-Power Hydrogen Arcjet," AIAA Paper 96-3183, July 1996.

A. C. Tribble
Associate Editor